Calculating Reachable Workspace Volume for Use in Quantitative Medicine

Robert Peter Matthew[1(✉)], Gregorij Kurillo[1], Jay J. Han[2], and Ruzena Bajcsy[1]

[1] Department of Electrical Engineering and Computer Science, University of California, Berkeley, Berkeley, CA, USA
{rpmatthew,gregorij,bajcsy}@eecs.berkeley.edu
[2] Department of Physical Medicine and Rehabilitation, University of California, Davis, Sacramento, CA, USA
jay.han@ucdmc.ucdavis.edu

Abstract. Quantitative measures of the space an individual can reach is essential for tracking the progression of a disease and the effects of therapeutic intervention. The reachable workspace can be used to track an individuals' ability to perform activities of daily living, such as feeding and grooming. There are few methods for quantifying upper limb performance, none of which are able to generate a reachable workspace volume from motion capture data. We introduce a method to estimate the reachable workspace volume for an individual by capturing their observed joint limits using a low cost depth camera. This method is then tested on seven individuals with varying upper limb performance. Based on these initial trials, we found that the reachable workspace volume decreased as muscular impairment increased. This shows the potential for this method to be used as a quantitative clinical assessment tool.

Keywords: Kinect · Muscular dystrophy · Functional workspace · Rehabilitation · Assessment · Diagnosis · Goniometry · Skeletal modelling

1 Introduction

Injury to the skeletal and muscular structure of an individual can occur through a variety of conditions ranging from traumatic accidents to genetic disorders. Monitoring the improvement of an individual's performance through medical treatments such as pharmaceuticals and rehabilitation, as well as tracking degeneration are key for customising medical treatment to an individual.

Traditional methods to track an individual's performance often relies on a series of qualitative tests administered by a clinical evaluator. These can range from recording the time to complete a specific task, to questionnaires and scored worksheets that measure quality of life.

However, a majority of these measures have focused on lower limb function, measuring an individual's performance when walking and climbing stairs.

L. Agapito et al. (Eds.): ECCV 2014 Workshops, Part III, LNCS 8927, pp. 570–583, 2015.
DOI: 10.1007/978-3-319-16199-0_40

There are relatively few methods for evaluating upper limb function, even though the upper limbs are critical for basic self-care activities. These activities are known as *Activities for Daily Living* or ADLs, and cover feeding, grooming, dressing and toileting care. Additionally, the need for quantitative measures for the upper limbs that are practical to implement, intuitive and scalable, has been echoed by medical practitioners.

We introduce a novel technique to quantify, the space an individual can reach using low cost sensing. By capturing an individual's upper limb motions while performing a set of arm movements that encompass cardinal shoulder range of motion, we introduce a method for creating an individualised skeleton, allowing calculation of their range of motion about each joint. These joint constraints are then used to find the region of space that the individual should be able to reach, centered at the shoulder. We call this the reachable workspace of the individual. Both the joint bounds and the volume of this reachable workspace, can be quantified and may act as usable clinical measures.

We evaluate the efficacy of these measures on a control population as well as a set of patients suffering from a degenerative neuromuscular disorder, comparing our measures to those typically used.

2 Related Work

Traditional methods for assessing limb function look at goniometry [1,2], muscle strength tests [3,4], clinical motor function scoring methods such as the Brooke, DASH and Fugl-Meyer scales [5–8] and performance based measures such as the 'nine hole peg test' and 'six minute walk test' [9–12].

The introduction of the Kinect depth camera [13] allowed for low cost, markerless motion capture with skeletal tracking. It has been used for goniometry [14,15] and tested against other motion capture devices to check its suitability for use as a clinical tool [16,17]. This has led to its use for rehabilitation measurement and exercise monitoring [18–23].

The reachable workspace of an individual has been measured for use in ergonomic design [24–26]. It has been extended for use as a clinical measure by combining it with traditional goniometry measures [27,28] and motion capture systems [29–32]. We extend this work by performing automated skeletal and goniometric measurements of the upper limb using the Kinect sensor, and calculating to creating a reachable workspace volume.

3 Mathematical Framework

In this section we introduce the mathematical tools we will use for recovering reachable workspace volume. We use techniques taken from robotics and computer graphics literature, particularly work in kinematic chains, state estimation and computational geometry [33,34]. Our method builds on the intuition that for every movement of the human arm, there is corresponding set of joint angles that describe this motion. By finding the bounds of these joint angles, we find the corresponding reachable volume in the world frame.

3.1 Kinematic Chains, Maps and Spaces

To build up the framework to describe these operations, we construct a kinematic chain that describes the arm. A kinematic chain is a set of rigid bodies, connected together by joints. Consider, the planar kinematic chain shown in Figure 1a. This chain comprises of two links, and two joints labelled J_j for $j \in [1, n]$ where n is the number of joints in the system.

We will perform our analysis based on the mappings between three separate spaces: configuration space$\mathcal{C}$, workspace $\mathcal{W}$ and outputspace $\mathcal{O}$. Our configuration space $\mathcal{C}$, is the space of all potential joint states. In our example, it is the set of angles $\theta_j \in [-\pi, +\pi]$ for $j \in [1, n]$.

For every combination of these joint angles, there is a corresponding (x, y) position of the kinematic chain. The mapping from the configuration space to the Cartesian space is given by the *forward kinematic map*, $f(\bar{\eta}, \boldsymbol{q})$ where $\bar{\eta}$ are the kinematic parameters of the model (such as joint lengths) and $\boldsymbol{q}$ is a vector of joint states. The image of f the workspace of the manipulator, denoted $\mathcal{W}$.

The manipulator workspace is contained in a larger 'output space' $\mathcal{O}$ which is the ambient space of smallest dimension that contains the workspace. We denote the m dimensional output space as $\mathcal{O}(m)$. In our example, we can take m as being either 2 or 3. $\mathcal{O}(2)$ would correspond to planar motion without orientation information $\left(\mathbb{R}^2\right)$, while $\mathcal{O}(3)$ would correspond to planar motion with orientation information $\left(\mathbb{R}^2 \times SO(2)\right)$.

The relationship between the configuration, work and output spaces and the forward kinematic map can therefore be summarised by the statement:

$$f(\bar{\eta}, \boldsymbol{q}) : \mathcal{C} \rightarrow \mathcal{W} \in \mathcal{O}$$

3.2 Constrained Kinematic Chains

In our previous example, we took each joint to be perfectly revolute with its domain being the circle. We now restrict the state of each joint J_j to remain in the bounded interval $\left[\underline{q}_j, \overline{q}_j\right]$ such that every state $q_j \in \left[\underline{q}_j, \overline{q}_j\right]$ for $j \in [1, n]$. We do this for both revolute and prismatic joints constructing $\boldsymbol{Q} \in \mathbb{R}^{n \times 2}$ an array containing the bounds of each joint such that $\boldsymbol{Q}_j = \left[\underline{q}_j, \overline{q}_j\right]$.

Under the assumption that these joint bounds are capable of completely characterising the reachable workspace, we can generate a set of feasible joint angles that lie within our configuration space. For every vector $\boldsymbol{q}_r \in \mathcal{C}$, we can say:

$$\boldsymbol{q}_r = [q_{1,r}, q_{2,r}, \ldots q_{j,r}, \ldots q_{n,r}] \text{ such that } q_{j,r} \in \left[\underline{q}_{j,r}, \overline{q}_{j,r}\right]$$

We can then use our forward kinematic map to relate a point $\boldsymbol{q}_r \in \mathcal{C}$ to a point $y_r \in \mathcal{O}$.

We make the assumption that as this point satisfies our joint bounds, it lies within our valid configuration space. This means that the point y_r is a valid point in our workspace $\mathcal{W}$.

Returning to our example, we can sample 1,000 feasible points in our output space (Figure 1b)) by mapping 1,000 feasible points from our configuration space. Alpha shapes [35] can be generated for these points allowing the non-convex hull of these points to be found as shown in Figure 1c.

To compare the validity of this method, we compare our recovered workspace to one that has been created analytically[34,36]. While the analytical solution is the ideal solution that we wish to find, the calculation becomes non-trivial for larger more complicated kinematic chains leading to use of our sampling based method.

4 Methodology

In this section, we outline the methods we used to build a skeleton for the individual and estimate the states and joint ranges for an observed motion.

We initially capture the actions of an individual performing actions relevant to ADLs. From this, we extract a kinematic model that captures the skeletal lengths and the joint range of motion. We then show how we estimate the workspace and reachable volume using these joint bounds.

4.1 Motion Capture

For our experiments, we used a Kinect depth camera to track the motions of an individual. We used the Microsoft Kinect SDK to extract the positions of several key points including the position of the head, shoulders, elbows, wrists and hips. The motion of the upper arm was recorded while the subject performed a set of prescribed movements. The 3D Cartesian coordinates for each of these points in the world frame were captured and stored.

4.2 Skeletonisation

To perform our analysis, we require a kinematic chain model of the upper arms. We used the coordinate convention outlined by the International Society of Biomechanics [37] to define a set of axes for the upper arm. This was then used to make a kinematic model of the upper arm (Figure 2).

The final model is a seven Degree of Freedom (DoF) chain, with the Glenohumeral (Gh) joint floating in space. The 6 DoF pose of the Gh centre represents the first six states in our state configuration vector $\boldsymbol{q}$. Our final state q_7 is the rotation of the Humeroulnar (Hu) joint.

This model requires two kinematic parameters- the length between the Gh and Hu joints and the length between the Hu and wrist. These lengths were taken to be the average length between the shoulder and elbow, and elbow and wrist respectively from the Kinect dataset. Given these two parameters the position of the shoulder, elbow and wrist are functions of the seven states $\boldsymbol{q}$.

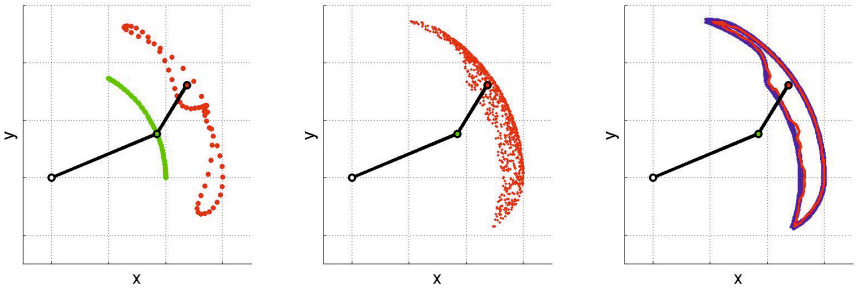

Fig. 1. Our methodology applied to a simple two link pantograph robot. Left: the robot performs an action, and the positions of the middle and end link are recorded (green and red points respectively). The joint angles corresponding to these points are found and then used to find the joint limits. Middle: These joint limits are used to find 1,000 feasible points in the output space (red). Right: The alpha-shape of these points is then found and taken to be the reachable workspace (red). This is compared to the reachable workspace calculated analytically (blue).

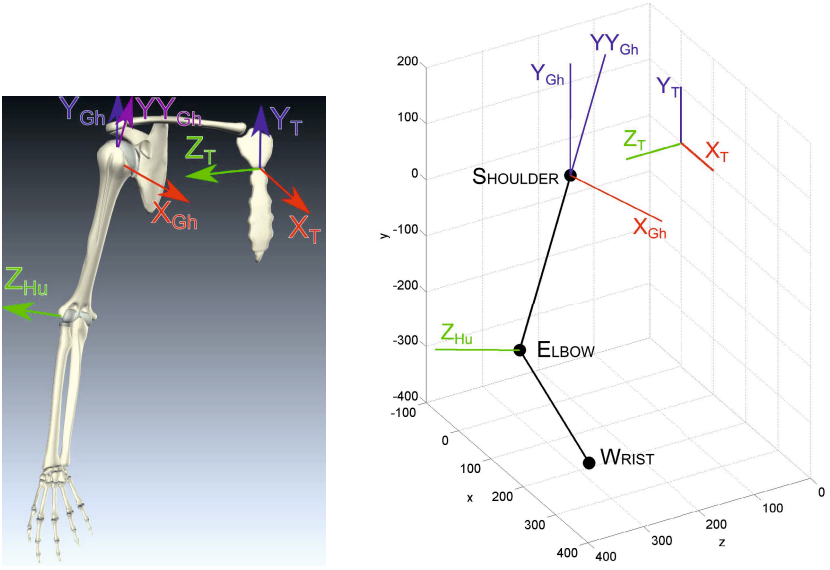

Fig. 2. Left: ISB recommendations on definitions of joint coordinates and rotational axes. Skeletal model generated using Biodigital Human[38]. Right: Our Kinematic model for the upper limbs. Y_{Gh} is parallel to Y_T, while YY_{Gh} runs parallel to the humerus. Location of the rotational centre of the Gh joint is given in Thorax (T) coordinates. Rotational pose of the Humerus is based on a Y-X-Y rotational sequence about Y_{GH}-X_{GH}-YY_{GH}. Rotation about the Hu joint is about the Hu_Z axis.

4.3 State Estimation

To capture the joint parameters of the individual, we need to find the observed range of states $\boldsymbol{q}$. However the Kinect only provides (noisy) shoulder, elbow and wrist positions. Given these observed trajectories $\boldsymbol{y}(t)$, we wish to find the corresponding state trajectories $\boldsymbol{q}(t)$.

To do this, we used an Unscented Kalman Filter (UKF) [39,40] to reconstruct the joint angles from the tracked data points [41]. Given a dynamic and observation model along with uncertainty parameters, this method can be used to estimate the state of a dynamic system. The UKF takes a discrete dynamical model of the form:

$$\boldsymbol{q}_{k+1} = F(\boldsymbol{q}_k, \boldsymbol{v}_k)$$

with the observation equation:

$$\boldsymbol{y}_k = H(\boldsymbol{q}_k, \boldsymbol{w}_k)$$

Ordinarily, we would create a dynamical system model for F, encapsulating the masses, inertias and torques being applied to the system. However in a biological system, this is often not known a priori. While tabulated values could be used as an estimate, the masses and inertias of body segments may vary heavily with medical pathology. Similarly, joint torque estimation is non-trivial, often requiring extensive musculoskeletal modelling.

Instead we drive our dynamical system with a random walk process, modelling the higer order dynamics as an Independent and Identically Distributed (I.I.D.) process [41].

In this manner we have a system model that will estimate our joint states $\boldsymbol{q}_k$ based on our observed measurements $\boldsymbol{y}_{1-k}$. In our experiments $\boldsymbol{y}$ is a $\mathbb{R}^{r\times 9}$ vector where r is the total number of samples, and our nine columns represent the Cartesian coordinates for the shoulder, elbow and wrist.

The UKF was run recursively on the Kinect dataset, removing segments of unreliable data. Data was deemed to be unreliable if the instantaneous change in angle exceeded 2 radians between two consecutive samples. The UKF was then reinitialised after this removal of data using the previous state values as the new starting guess.

The recovered state values were then passed through a zero-phase 3^{rd} order lowpass Butterworth filter[42] with a normalised cutoff frequency of 0.1.

The maximum and minimum values $\left(\underline{q}_j, \overline{q}_j\right)$ for each joint j were calculated and stored as in the bounding matrix $\boldsymbol{Q}$.

4.4 Workspace Generation

Using these bounds, we can create random joint angles respecting the bounds via an I.I.D. process. In this manner, we generate 10,000 sample points in configuration space $\left(\boldsymbol{q}^{7\times 10{,}000}\right)$, which were then mapped into 10,000 wrist positions in our output space $\left(\boldsymbol{y}^{3\times 10{,}000}\right)$.

While these points marked out valid regions in our workspace, we require a volumetric measurement of our reachable workspace. Using this point cloud of feasible workspace points, we used alpha-shapes[35] to create a non-convex hull marked out by this sampled data. The enclosed volume of this hull was then used as our recovered reachable workspace volume.

5 Experimental Validation

To evaluate the validity of this method, we recorded Kinect joint positions for both pathological and control test subjects. We outline our subject population and the experimental procedure and show the results from our method.

5.1 Experimental Population

Four patients diagnosed with Facioscapulohumeral muscular dystrophy (FSHD) and three healthy controls participated in this initial study. FSHD patients were diagnosed based on confirmed genetic analysis as fully described in [32]. Healthy control subjects without any musculoskeletal disorders were recruited through an approved Institutional Review Board (IRB) protocol. Consent was obtained prior to the study for all participants or their guardians and was documented via an IRB approved consent form.

FSHD is a genetic disease of skeletal muscle that stereotypically affects the skeletal muscles of the face and the shoulder girdle. Symptoms begin in early childhood with proximal upper limb muscle impairment, and progress through the teenage years. Life expectancy is unaffected, but often results in severe disabilities eventually requiring wheelchair use.

Current methods of assessing FSHD are the Brooke scale, a specific FSHD scale, shoulder-elbow strength measurements, 9-hole pegboard tests, and quality of life questionnaires. Of these, the Brooke scale is one of the most commonly used and will be used as our measure of comparison.

5.2 Experimental Procedure

Participants in the study were asked to perform a series of motions that marked out key points of their workspace. They were asked to touch six points on their body, the left and right sides of their hips, their left and right shoulders, their mouth and the top of their head while being monitored by a Kinect camera. These actions were chosen as it covers areas necessary for ADLs such as eating, grooming and toileting and covers motion in clinically relevant planes. Each pathological participant was also given a Brooke score by the study clinical evaluator.

5.3 Reachable Volume Results

We used our method for reconstructing the reachable workspace and calculating the reachable volume, one each of our participants. The results of these trials are shown in Table 1, with graphical depictions of these workspaces for a healthy subject and a subject with progressed FSHD shown in Figures 3-6.

Table 1. Comparison of computed reachable volume and Brooke Score

Subject	Reachable Volume (m^3)	Brooke Score (unitless)
Healthy 1	3.74×10^{-1}	-
Healthy 2	3.28×10^{-1}	-
Healthy 3	2.34×10^{-1}	-
Patient 1	3.58×10^{-1}	1
Patient 2	2.70×10^{-1}	2
Patient 3	1.78×10^{-1}	3
Patient 4	1.48×10^{-3}	5

6 Discussion

From the results shown in Table 1, we can see that as the Brooke score increases (showing increasing disability), the computed reachable volume decreases. Patients with low levels of disability have reachable volumes on par with that of the healthy individuals.

Looking qualitatively at the reachable workspace for the healthy and impaired subjects (Figures 3-6), we can see that there are distinct changes in the shape of the reachable workspace with change in Brooke score.

The reachable workspace for the healthy individual matches the reachable workspaces seen in previous studies [27]. The reachable space respects observed

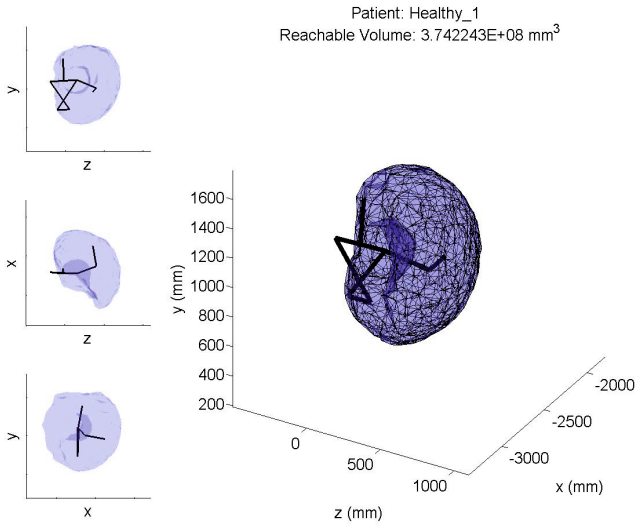

Fig. 3. Reachable workspace for a healthy subject. Upper extremities are shown in wire-frame with the reachable workspace shown in blue. Plane projected views are shown on the left.

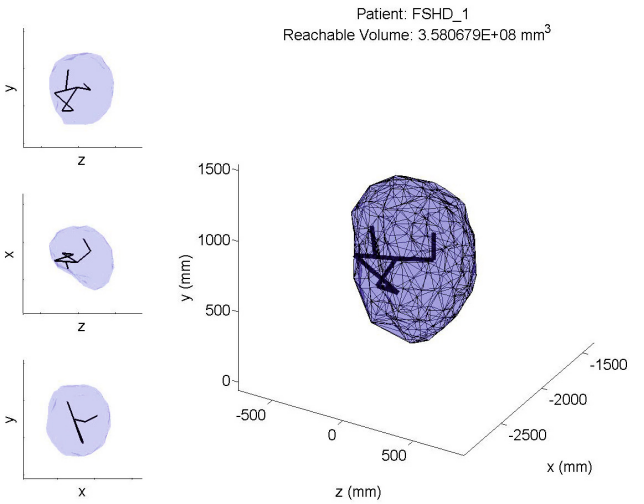

Fig. 4. Reachable workspace for Patient 1 with mild FSHD (Brooke 1)

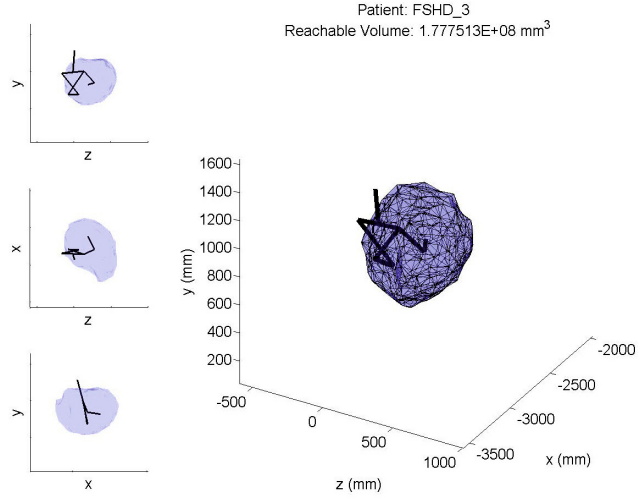

Fig. 5. Reachable workspace for Patient 3 with moderate FSHD (Brooke 3)

physiological limitations; the wrist is unable to contact the shoulder centre and there is a section of space behind the individual that is unreachable.

As the Brooke score increases, the computed reachable workspace decreases. This decrease is seen most notably in the vertical (y) direction, with the workspace no longer reaching the top of the head in Figure 5, and being level with the waist in Figure 6. This gives an indication of what is and is not possible for the individual suggesting which patients are able to perform which ADLs.

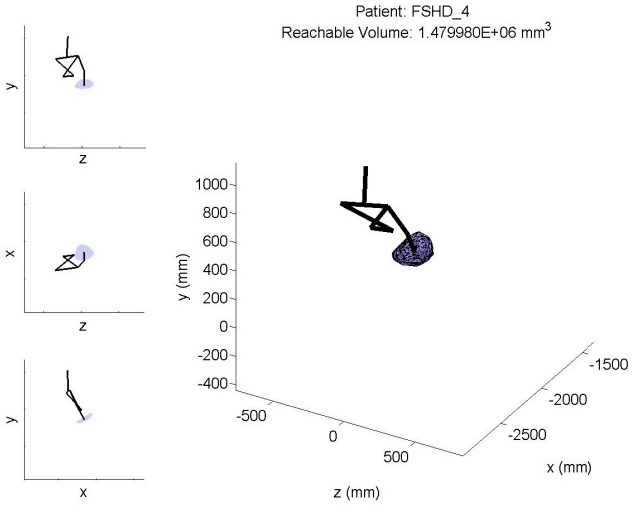

Fig. 6. Reachable workspace for patient 4 with severe FSHD (Brooke 5)

While the population size used is small, it does suggest that our quantified measure *reachable workspace volume* may be an effective method for assessing patients with FSHD and various other neuromusculoskeletal conditions, potentially characterising performance at a higher fidelity than existing methods.

6.1 Limitations

There are a number of important limitations in both our method and experimental procedure.

To generate our estimate of the reachable workspace, we make two assumptions. The first is that each joint can be taken to be independent of another. The second assumption is that the workspace is only limited by these joint bounds. These are two significant simplifications of a true system. In biological musculoskeletal structures, there are *biarticular* muscles whereby muscles span several joints. As the total length of this muscle is limited, the angles of the joints that it spans are related to each other. Similarly the shoulder complex has a number of physical constraints of the pose of the Gh centre with respect to the torso. Our second assumption works under the premise that the joint bounds can completely characterise the reachable workspace. Any workspace reduction due to muscle weakness is characterised by the respective joint angles and is independent of end point position.

We also assume that an individual reaches their joint limits when performing the motion capture task. The computed results for our healthy subjects may suggest that these joint limits were not seen, resulting in lower than expected reachable volumes.

Furthermore, these reachable volumes were not scaled to the individual. Individuals with longer arms will have a larger reachable volume given the same joint limitations. This makes the comparison between individuals using a non-normalised reachable volume potentially misleading.

Finally this is a sampling based method that relies on finding representative workspace points through random sampling. This process is computationally taxing, and does not guarantee that the found volume will accurately describe the true workspace. While the method provided representative results when compared to the analytical solution in our planar example (Figure 1), this performance needs to be accurately evaluated.

6.2 Future Work

The work presented here represents our initial findings as part of a larger study. We seek to apply these methods to a larger population set, within the FSHD community as well as for evaluating rehabilitative performance. Furthermore, the repeatability and reliability of these measures needs to be investigated as well as comparison to the conventional methods for clinical assessment.

In our method we calculated joint bounds Q that were used to represent an individuals' abilities. The study of how these angles vary with FSHD progression, as well as creating assessment measures that combine both joint angle and reachable volume may help to further quantify performance.

7 Appendix

7.1 Brooke Scale

The Brooke Scale can be summarised as showing in Table 2.

Table 2. Brooke Scoring for the Upper Limbs[5]

Brooke Score	Description
1	Starting with arms at sides, abduct arms in a full circle until they touch above the head.
2	Can raise arms above head only by shortening the arc of motion or using accessory muscles.
3	Cannot raise hands above head but can raise an 8oz. glass/cup of water to mouth (using both hands if necessary).
4	Can raise hands to mouth but cannot raise an 8 oz. glass/cup of water to mouth.
5	Cannot raise hand to mouth but can use hands to hold pen or pick up pennies from table.
6	Cannot raise hands to mouth and has no useful function of hands.

References

1. Gajdosik, R.L., Bohannon, R.W.: Clinical measurement of range of motion: Review of goniometry emphasizing reliability and validity. Physical Therapy **67**(12), 1867–1872 (1987)
2. Macedo, L.G., Magee, D.J.: Differences in range of motion between dominant and non-dominant sides of upper and lower extremities. Journal of manipulative and physiological therapeutics **31**(8), 577–582 (2008)
3. Bohannon, R.: Manual muscle test scores and dynamometer test scores of knee extension strength. Archives of physical medicine and rehabilitation **67**(6), 390–392 (1986)
4. Escolar, D., Henricson, E., Mayhew, J., Florence, J., Leshner, R., Patel, K., Clemens, P.: Clinical evaluator reliability for quantitative and manual muscle testing measures of strength in children. Muscle & nerve **24**(6), 787–793 (2001)
5. Brooke, M.H., Griggs, R.C., Mendell, J.R., Fenichel, G.M., Shumate, J.B., Pellegrino, R.J.: Clinical trial in duchenne dystrophy. i. the design of the protocol. Muscle & nerve **4**(3), 186–197 (1981)
6. Beaton, D.E., Katz, J.N., Fossel, A.H., Wright, J.G., Tarasuk, V., Bombardier, C.: Measuring the whole or the parts?: Validity, reliability, and responsiveness of the disabilities of the arm, shoulder and hand outcome measure in different regions of the upper extremity. Journal of Hand Therapy **14**(2), 128–142 (2001). The Outcome Issue
7. Lamperti, C., Fabbri, G., Vercelli, L., D'Amico, R., Frusciante, R., Bonifazi, E., Fiorillo, C., Borsato, C., Cao, M., Servida, M., et al.: A standardized clinical evaluation of patients affected by facioscapulohumeral muscular dystrophy: The fshd clinical score. Muscle & nerve **42**(2), 213–217 (2010)
8. Fugl-Meyer, A.R., Jääskö, L., Leyman, I., Olsson, S., Steglind, S.: The post-stroke hemiplegic patient. 1. a method for evaluation of physical performance. Scandinavian journal of rehabilitation medicine **7**(1), 13–31 (1974)
9. Mathiowetz, V., Weber, K., Kashman, N., Volland, G.: Adult norms for the nine hole peg test of finger dexterity. Occupational Therapy Journal of Research (1985)
10. Sharpless, J.: The nine hole peg test of finger hand coordination for the hemiplegic patient. Mossman's A Problem Orientated Approach to Stroke Rehabilitation (1982)
11. Duncan, P.W., Weiner, D.K., Chandler, J., Studenski, S.: Functional reach: A new clinical measure of balance. Journal of Gerontology **45**(6), M192–M197 (1990)
12. Enright, P.L.: The six-minute walk test. Respiratory care **48**(8), 783–785 (2003)
13. Zhang, Z.: Microsoft kinect sensor and its effect. IEEE MultiMedia **19**(2), 4–10 (2012)
14. Bo, A., Hayashibe, M., Poignet, P., et al.: Joint angle estimation in rehabilitation with inertial sensors and its integration with kinect. In: EMBC 2011: 33rd Annual International Conference of the IEEE Engineering in Medicine and Biology Society, pp. 3479–3483 (2011)
15. Fern'ndez-Baena, A., Susin, A., Lligadas, X.: Biomechanical validation of upper-body and lower-body joint movements of kinect motion capture data for rehabilitation treatments. In: 2012 4th International Conference on Intelligent Networking and Collaborative Systems (INCoS), pp. 656–661, September 2012
16. Chang, C.Y., Lange, B., Zhang, M., Koenig, S., Requejo, P., Somboon, N., Sawchuk, A., Rizzo, A.: Towards pervasive physical rehabilitation using microsoft kinect. In: 2012 6th International Conference on Pervasive Computing Technologies for Healthcare (PervasiveHealth), pp. 159–162, May 2012

17. Khoshelham, K., Elberink, S.O.: Accuracy and resolution of kinect depth data for indoor mapping applications. Sensors **12**(2), 1437–1454 (2012)
18. Chang, Y.J., Chen, S.F., Huang, J.D.: A kinect-based system for physical rehabilitation: A pilot study for young adults with motor disabilities. Research in Developmental Disabilities **32**(6), 2566–2570 (2011)
19. Lange, B., Chang, C.Y., Suma, E., Newman, B., Rizzo, A., Bolas, M.: Development and evaluation of low cost game-based balance rehabilitation tool using the microsoft kinect sensor. In: 2011 Annual International Conference of the IEEE Engineering in Medicine and Biology Society, EMBC, pp. 1831–1834, August 2011
20. Lange, B., Koenig, S., McConnell, E., Chang, C., Juang, R., Suma, E., Bolas, M., Rizzo, A.: Interactive game-based rehabilitation using the microsoft kinect. In: Virtual Reality Short Papers and Posters (VRW), pp. 171–172, 2012 IEEE, March 2012
21. Pastor, I., Hayes, H., Bamberg, S.: A feasibility study of an upper limb rehabilitation system using kinect and computer games. In: Engineering in Medicine and Biology Society (EMBC), 2012 Annual International Conference of the IEEE, pp. 1286–1289, August 2012
22. Uzor, S., Baillie, L.: Exploring & designing tools to enhance falls rehabilitation in the home. In: Proceedings of the SIGCHI Conference on Human Factors in Computing Systems. CHI 2013, pp. 1233–1242. ACM, New York (2013)
23. Anton, D., Goni, A., Illarramendi, A., Torres-Unda, J., Seco, J.: Kires: A kinect-based telerehabilitation system. In: 2013 IEEE 15th International Conference on e-Health Networking, Applications Services (Healthcom), pp. 444–448, October 2013
24. Li, S., Xi, Z.: The measurement of functional arm reach envelopes for young chinese males. Ergonomics **33**(7), 967–978 (1990)
25. Book, A.S.: Vol. 1: Anthropometry for designers. NASA Reference Publication 1024 (1978)
26. Sengupta, A.K., Das, B.: Maximum reach envelope for the seated and standing male and female for industrial workstation design. Ergonomics **43**(9), 1390–1404 (2000)
27. Klopčar, N., Lenarčič, J.: Kinematic model for determination of human arm reachable workspace. Meccanica **40**(2), 203–219 (2005)
28. Klopčar, N., Tomšič, M., Lenarčič, J.: A kinematic model of the shoulder complex to evaluate the arm-reachable workspace. Journal of biomechanics **40**(1), 86–91 (2007)
29. Kurillo, G., Han, J.J., Obdrzálek, S., Yan, P., Abresch, R.T., Nicorici, A., Bajcsy, R.: Upper extremity reachable workspace evaluation with kinect. In: MMVR, pp. 247–253 (2013)
30. Kurillo, G., Han, J., Nicorici, A., Johnson, L., Abresch, R., Henricson, E., McDonald, C., Bajcsy, R.: Upper extremity reachable workspace evaluation in DMD using kinect. Neuromuscular Disorders **23**(910), 749–750 (2013). 18th International Congress of The World Muscle Society
31. Kurillo, G., Chen, A., Bajcsy, R., Han, J.J.: Evaluation of upper extremity reachable workspace using kinect camera. Technology and Health Care **21**(6), 641–656 (2013)
32. Han, J.J., Kurillo, G., Abresch, R.T., de Bie, E., Nicorici, A., Bajcsy, R.: Reachable workspace in facioscapulohumeral muscular dystrophy (fshd) by kinect. Muscle & nerve (2014)
33. Siciliano, B., Khatib, O.: Springer Handbook of Robotics. Springer (2008)

34. Khalil, W., Dombre, E.: Modeling. Butterworth-Heinemann, Identification and Control of Robots (2004)
35. Edelsbrunner, H., Mücke, E.P.: Three-dimensional alpha shapes. ACM Trans. Graph. **13**(1), 43–72 (1994)
36. Burdick, J.W.: Kinematic Analysis and Design of Redundant Robot Manipulators. PhD thesis, Stanford University (1988)
37. Wu, G., Van Der Helm, F.C., Veeger, H., Makhsous, M., Van Roy, P., Anglin, C., Nagels, J., Karduna, A.R., McQuade, K., Wang, X., et al.: Isb recommendation on definitions of joint coordinate systems of various joints for the reporting of human joint motionpart ii: Shoulder, elbow, wrist and hand. Journal of biomechanics **38**(5), 981–992 (2005)
38. Biodigital: Biodigital human (06 2014)
39. Julier, S.J., Uhlmann, J.K.: A new extension of the kalman filter to nonlinear systems. In: Int. symp. aerospace/defense sensing, simul. and controls. vol. 3, pp. 3–2, Orlando (1997)
40. Wan, E.A., Van Der Merwe, R.: The unscented kalman filter for nonlinear estimation. In: Adaptive Systems for Signal Processing, Communications, and Control Symposium 2000. AS-SPCC. The IEEE 2000, pp. 153–158. IEEE (2000)
41. Ziegler, J., Nickel, K., Stiefelhagen, R.: Tracking of the articulated upper body on multi-view stereo image sequences. In: 2006 IEEE Computer Society Conference on Computer Vision and Pattern Recognition, vol. 1, pp. 774–781, June 2006
42. Butterworth, S.: On the theory of filter amplifiers. Wireless Engineer **7**, 536–541 (1930)